THE JOURNAL OF PHYSICAL CHEMISTRY C

pubs.acs.org/JPCC Article

Small Thiols Stabilize the Shape of Gold Nanorods

Sonia Centi, Lucia Cavigli, Claudia Borri, Alessio Milanesi, Martina Banchelli, Sofia Chioccioli, Boris N. Khlebtsov, Nikolai G. Khlebtsov, Paolo Matteini, Patrizia Bogani, Fulvio Ratto,* and Roberto Pini

Cite This: https://dx.doi.org/10.1021/acs.jpcc.0c00737 Read Online

ACCESS | Metrics & More | Article Recommendations | Supporting Information

ABSTRACT: The stabilization of the optical properties of anisotropic plasmonic particles upon thermal annealing and laser irradiation is an important issue in many biomedical applications. Here, we address the effect of small thiols on the thermal and photostability of gold nanorods. As-synthesized colloids were treated with mixtures of thiolated polyethylene glycol and methylbenzenethiol with molar ratios ranging from 0, for pure PEG, to 20 and then incubated in an oven at sub-boiling conditions. We found that small thiols dramatically enhance the thermal stability of gold nanorods. For instance, after 1 h at 90 °C samples with pure PEG lost more than 70% of optical absorbance at their initial peak position, while particles coated with a thicker layer of methylbenzenethiol remained nearly unchanged. We ascribe this effect to a modulation of the activation barrier for surface diffusion of gold atoms. Additionally, we addressed the translation of this effect to the photostability of gold nanorods irradiated under conditions of interest in photoacoustic imaging and found that small thiols delay relevant damage thresholds by as much as a factor of 2. Our findings will help researchers design novel tags that overcome the limitations related to thermal and photoinstabilities in a broad variety of applicative contexts.

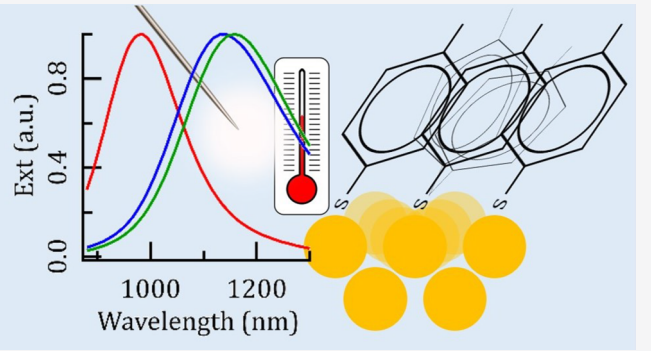

INTRODUCTION

Over the past couple of decades or so, near-infrared resonant plasmonic particles exhibiting conformational anisotropy have received substantial interest for applications as contrast agents in biomedical optics.[1−6] In some cases, their use has literally accompanied the emergence of major innovations, such as photoacoustic imaging[7−9] and flow cytometry,[10,11] where these materials have appeared ever since seminal papers. In these contexts, the optimization of their photostability is a recurrent issue[10,12−19] because, in most cases of practical interest, relevant thresholds fall well below maximum permissible exposure (MPE) boundaries[20] and so represent a limiting factor. Even at room temperature,[21] but much more prevalently upon irradiation with short optical pulses, noble-metal particles start to premelt through a process of atomic surface diffusion that requires no phase transition, proceeds with thermal activation through Arrhenius behavior,[21−24] and promotes a collective reconfiguration that tends to lower their surface to volume ratio, that is, to gain higher sphericity.[25] The exact pathway behind this reconfiguration remains a subject of ongoing research. In the case of gold nanorods, most authors have postulated a gradual relocation of material from the end-caps to the side walls.[22,24,26] However, other authors have evoked more complex phenomena, such as the ejection of spherical fragments according to Rayleigh-Plateau instability,[27] as occur in metal wires[28,29] and liquid columns. In a recent paper,[23] we outlined a simple model for the kinetics of the transformation of gold nanorods where we implemented a constant value of 0.6 eV for the activation energy for atomic surface diffusion. However, an accurate description of this parameter needs to account for local details, such as curvature[22,24] or chemical coordination,[30−32] which make sharper tips more mobile, and environmental features, such as stiffness,[21,24] which modify the overall dynamics.

Among the strategies proposed to inhibit the effect of reshaping, the use of thick shells made of silica,[14,33] mixed Si−Ti oxide,[34] or organosilica[18] stands out as an effective tool that constrains the initial shape by acting as a rigid mold. As a rule of thumb, for instance, we quantified that the threshold of optical fluence for reshaping of gold nanorods increases by as much as 10% per nanometer of added organosilica.[18] However, this approach modifies the functionality of plasmonic particles in very many respects. In a sense, silanization may confer valuable porosity and tunable hydrophilicity for use, for

Received: January 27, 2020
Revised: April 29, 2020
Published: April 30, 2020

instance, to carry and enable the controlled release of drugs[33,35,36] or to host upconverting lanthanides for local thermometry.[37] In another sense, its effect may be intrusive and bring along significant drawbacks, in terms of much more complexity, cytotoxicity,[18] and a negative impact on near field-based applications, such as surface enhanced raman scattering (SERS) or colorimetric assays.

Here, we present a protocol that makes use of a small thiol to affect the kinetics of premelting of gold nanorods, and we assess its performance under conditions of practical relevance for applications in vitro and in vivo. The interaction between noble metal films or particles, small thiols, and their self-assembled monolayers has been the subject of extensive and ongoing research.[38−40] In particular, the adsorption and desorption of such species have been investigated under a broad variety of conditions.[41−48] What emerges is that denser layers of aromatic thiols supporting π-interactions tend to exhibit more stability[42−45,48] as a rule of thumb. However, much less attention has been paid to the other side of the interface, which may reveal more opportunities for technological applications. Our work fits in this gap. We postulate that thiolate-bound gold atoms are more constrained and exhibit higher activation energy for surface hopping,[30,32] thus delaying the onset of reshaping. We demonstrate this effect on the thermal stability of a colloidal suspension of gold nanorods left in an oven at moderate temperature and discuss its implication on their photostability under conditions of interest in photoacoustic imaging.

EXPERIMENTAL METHODS

Materials. α-Methoxy-ω-mercapto poly(ethylene glycol) (PEG, MW 5000 Da, mPEG-SH) was acquired from Iris Biotech GmbH (Marktredwitz, Germany). All other chemicals were purchased from Sigma-Aldrich (St. Louis, MO, U.S.A.) and used as received.

Synthesis of the Particles. Gold nanorods were synthesized according to our variant of the protocol developed by Vigderman and Zubarev.[49,50] After synthesis, particles were brought to a concentration of 1.6 mM Au in a 100 mM acetate buffer of pH 5.0 containing 500 μM cetrimonium bromide (CTAB) and 0.005% (w/w) polysorbate 20 and 50 μM mPEG-SH.[51] After 30 min under gentle agitation at 37 °C, suspensions were supplemented with different doses of methylbenzenethiol (MBT), that is, none (sample PEG/MBT 1:0), 50 μM (PEG/MBT 1:1), or 1 mM (PEG/MBT 1:20), and left at rest at 4 °C for 24 h. Finally, all particles were purified by three cycles of centrifugation, in order to remove the excess of free thiols, and transferred to ultrapure water containing 0.005% (w/w) polysorbate 20. The reaction buffer and the supernatant obtained after the first cycle of centrifugation were treated with Ellman's reagent, and their optical absorbance around 412 nm was compared in order to assess the percentage of unreacted thiols.

Optical and Morphological Characterization of the Particles. The PEGylation and collodial stability of the particles were checked by dynamic light scattering[52] with a Zetasizer Nano ZS 90 platform from Malvern Instruments (Malvern, U.K.). Spectra of optical extinction were recorded with a Lambda 950 spectrophotometer from PerkinElmer (Waltham, MA, U.S.A.). Optical spectra were analyzed with a numerical model that represents a convolution of a Weibull distribution of aspect ratio (AR, or ratio of length to diameter) times the line shape returned from the dipolar approximation of Mie-Gans theory.[53] Details are given elsewhere.[25,54] This model allows us to work out an effective distribution of AR from the optical spectra of gold nanorods or the refractive index of their medium. Since particles are rendered as spheroids, results fail to account for subtle details of their shape,[55] such as the precise layout of facets and so forth, and are approximate. However, the final outcome is often accurate to the level of a few percent[25] and succeeds to capture major trends involved in the process of reshaping.

SERS experiments were carried out using a Xplora microRaman spectrometer from Horiba (Villeneuve-d'Ascq, France) coupled to 532 or 785 nm wavelength laser sources. Single acquisitions were performed with integration time of 10 s, laser power at the sample of 4.8 mW, and a 1200-grooves/mm grating. The backscattered signal was acquired by means of a 10× microscope objective (0.25 NA), generating an ∼7 μm beam waist that provides an average response, in turn minimizing possible local signal variability. SERS measurements were performed by focusing the laser beam on the exposed face of a 7 μL droplet of suspended particles (PEG/MBT 1:0, 1:1, and 1:20) accommodated in 3 mm^2 round holes obtained from a polylpropylene support.[56] SERS data are reported as average over 15 random measurement points from 3 replicated samples.

Transmission electron micrographs were acquired in the laboratories of Center for Electronic Microscopy Laura Bonzi of CNR in Sesto Fiorentino with a CM12 platform from Philips (Amsterdam, The Netherlands) operated at 100 kV or at Simbioz Center for the Collective Use of Research Equipment in the Field of Physical−Chemical Biology and Nanobiotechnology of IBPPM RAS in Saratov with a Libra-120 transmission electron microscope from Carl Zeiss (Jena, Germany). For TEM measurements, suspensions of particles were centrifuged twice and resuspended in ultrapure water. Five microliters of samples were deposited onto 300-mesh copper grids covered with Formvar films and left to dry in an oven at 40 °C.

Photoacoustic Characterization of the Particles. Photoacoustic experiments were carried out with a homemade inverted photoacoustic microscope.[50,57] The optical source was a fiber-coupled diode-pumped microchip laser by Asclepion Laser Technologies (Jena, Germany) emitting pulses with a wavelength of 1064 nm, duration of 3.3 ns, and repetition rate of 10 Hz. An attenuator placed in front of the output was used to tune the optical fluence, which was monitored in real time with a QE8SP pyroelectric detector from Gentec-EO (Quebec, QC, Canada). Photoacoustic signals were acquired by an amplified immersion transducer from Olympus Panametrics (mod V382-SU-F, sensor diameter 0.5 in., frequency range 3.5 MHz, focal distance 0.83 in., 40 dB amplifier mod 5676, Tokyo, Japan) and recorded with a RTO1004 digital oscilloscope from Rohde&Schwarz (Munich, Germany).

Flow chambers (μ-Slide I Luer Family, channel height 200 μm, IBIDI GmbH, Planegg/Martinsried, Germany) were filled with suspensions of gold nanorods, coupled to a peristaltic pump (model FH10, Thermo Scientific, Waltham, MA U.S.A.), and immersed in DI water.[57] The use of microfluidic chambers is a promising tool to assess the performance of photoacoustic systems and contrast agents.[58,59] The laser beam was focused perpendicular to the flow chamber with a spot diameter of 300 μm.

Photoacoustic signals (I) were analyzed in terms of peak-to-peak amplitude and their trend with fluence of the optical

https://dx.doi.org/10.1021/acs.jpcc.0c00737
J. Phys. Chem. C XXXX, XXX, XXX−XXX

trigger (F) was modeled with an analytical function that describes a depletion of optical absorbance according to a sigmoid curve[18,23]

$$I = a + \frac{b \cdot F}{1 + \left(\frac{F}{F_0}\right)^p} \quad (1)$$

The parameters contained in the sigmoid term were worked out to extract a threshold for photoinstability as $F_{th} = (1/3)^{1/p} \cdot F_0$, which amounts to a loss of efficiency of photoacoustic conversion by 25%, consistent with our previous definition.[16,18,23]

RESULTS AND DISCUSSION

Model of Thiolated Particles. In order to assess the effect of small thiols on the stability of gold nanorods, we added different amounts of MBT to the reaction mixture used for their PEGylation. The latter probably represents the most standard modification of gold nanorods for applications in biomedical optics.[51,60−62] Figure 1a shows a representative transmission electron image of the particles used in this work. We chose MBT for its ability to form self-assembled monolayers[63−66] that change in conformation and stability with density due to the effect of π-stacking. In addition, benzene thiols are a common choice for use as reference for performance assessment of SERS substrates[67] or to prepare SERS tags for biomedical sensing.[68,69] Here, we treated as-synthesized gold nanorods with thiolated PEG and MBT at different molar ratios. We started with a rate of thiolated PEG/MBT of 1:0, which has no MBT but just our PEGylated benchmark. Next, the ratio was modified to 1:1, where the dosage of MBT was such that the nominal size of gold surface area available per small thiol was about 25−50 Å^2, and finally a ratio of 1:20, that is, a gold surface area per MBT molecule around 1.3−3 Å^2. Since the footprint of MBT in a self-assembled monolayer on gold is 19 Å^2,[70] the latter sample theoretically reflects a condition of oversaturation. Instead, the intermediate case stands below saturation. Note that we use the labels PEG/MBT 1:0, 1:1, and 1:20 in order to indicate these three cases according to their ratios of thiols dosed in the reaction mixture. The actual density of PEG and MBT immobilized on the particles is more difficult to determine. The quantification of thiols left unreacted in the reaction buffer suggests that sample 1:1 is close to the nominal density of MBT, and sample 1:20 reaches saturation and actually carries as much as 2−4 monolayers of MBT, probably stacked through hydrophobic interactions prior to subsequent purification. In practice, we consider sample 1:20 as the subject of our study, 1:0 as our benchmark, and 1:1 as an intermediate case used to verify the existence of a trend. Figure 1b provides a cartoon of our samples for use as a memo, where some details may be inaccurate. In particular, as we shall see, the persistence of PEG in the particles treated with MBT may be subject to dynamic thiol exchange. Conversely, different observations concur to confirm the trend in density of MBT bound per particle.

Figure 1c displays the spectra of optical extinction of our samples. We observed a red shift of the plasmonic bands upon increase in dosage of MBT with their longitudinal oscillations peaking from 1143 to 1167 to 1172 nm. We analyzed these spectra with a numerical model derived from Mie-Gans theory[53] that was demonstrated elsewhere[25,54] and double-checked once more in this work (see Supporting Information).

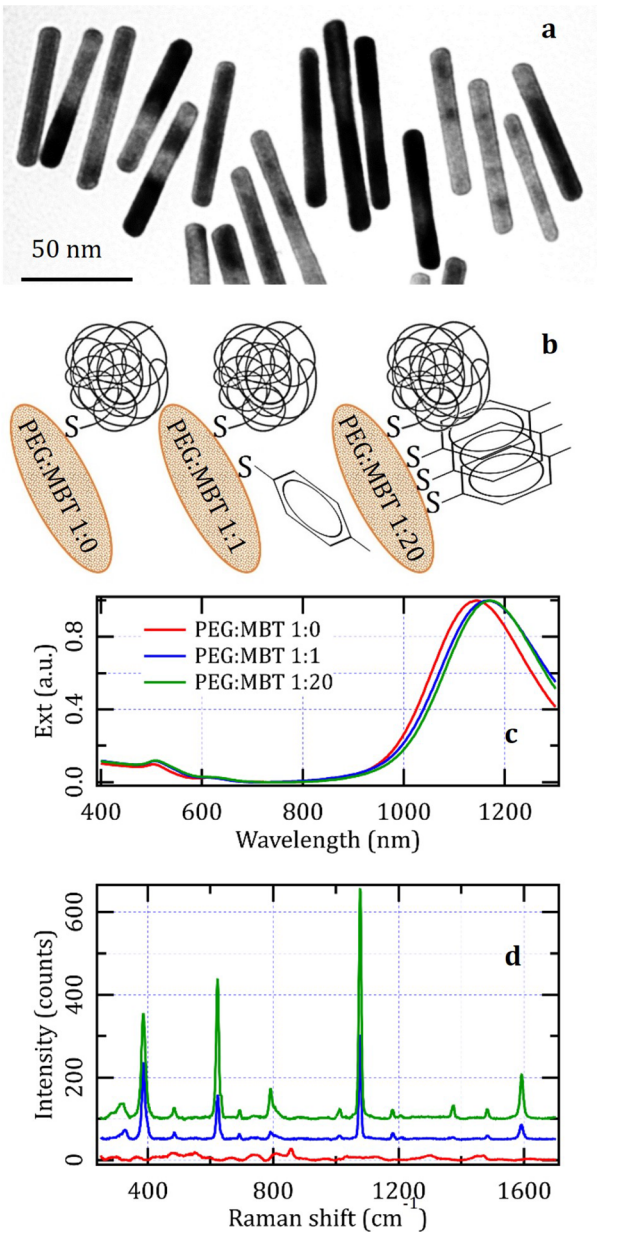

Figure 1. (a) Representative transmission electron micrograph of the particles used in the main text of this work. (b) Cartoon representing the different modifications with a ratio of PEG/MBT of 1:0, 1:1, or 1:20, from left to right. Methoxylated PEG is drawn as a curled strand. (c) Their spectra of optical extinction. (d) Their Raman spectra acquired with an excitation wavelength of 785 nm. Curves were offset by 50 counts for clarity.

According to this model, the optical features of our samples arise from a distribution of AR with an average of 7.7 and standard deviation of 0.8, and their shift points to an increase of effective refractive index from 1.33 to 1.36 to 1.37. A red shift of the plasmonic bands of gold nanospheres that tends to saturate with density of MBT was also reported by Lu et al.[71]

Figure 1d compares the Raman spectra of our samples. The Au−S modes around 380 cm^{-1} increase with dosage of MBT, which accounts for an overall enrichment in thiols anchored to the metal surface. The change of intensity ratio between the SERS bands corresponding to vibrational modes with in-plane A1 to out-of-plane B1 symmetry seen from sample PEG/MBT 1:1 to 1:20 suggests a compaction of the layer of MBT[71−74]

https://dx.doi.org/10.1021/acs.jpcc.0c00737
J. Phys. Chem. C XXXX, XXX, XXX−XXX

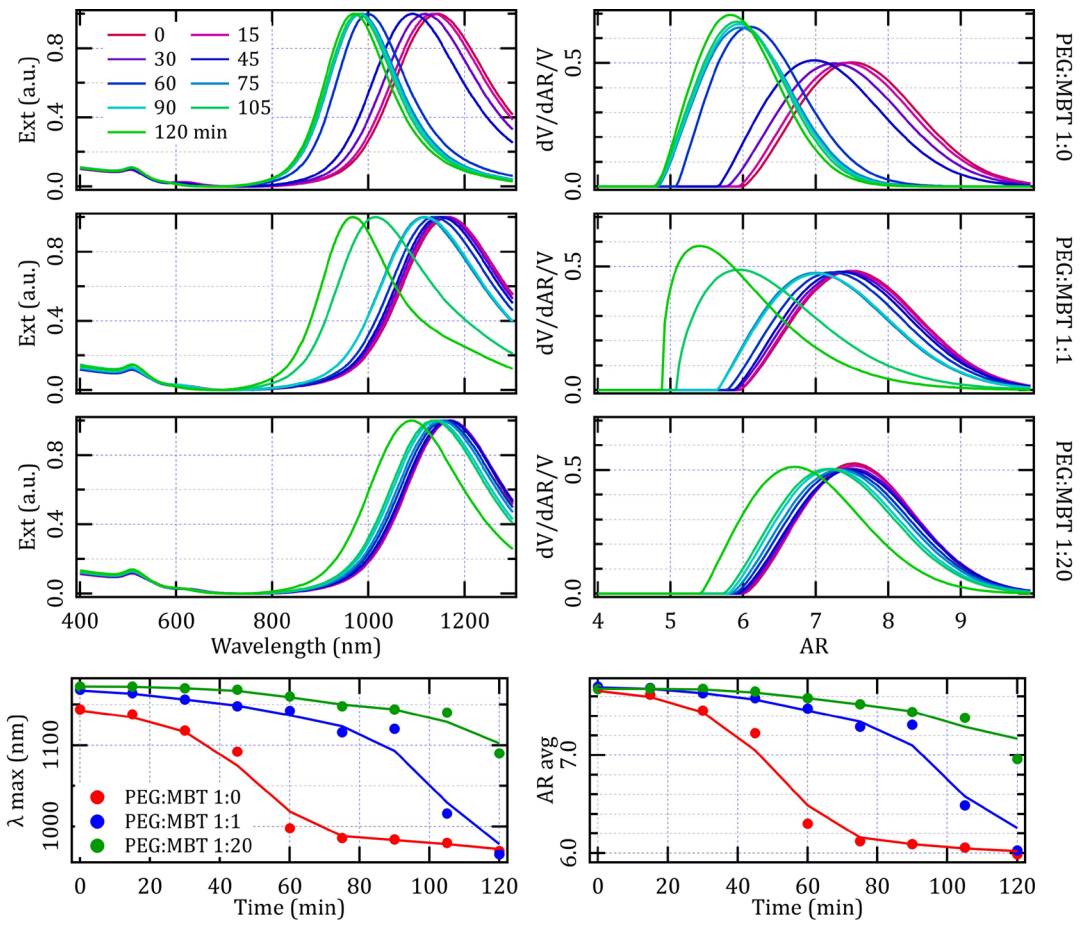

Figure 2. Normalized spectra of optical extinction and their decryption in terms of distributions of AR for particles modified with the named mixtures of thiols and treated for the named intervals at 90 °C. Note that the right-hand histograms integrate to unity. The lower panels summarize the kinetics of evolution of peak position of the longitudinal band and average value of AR: dots are experimental values; lines are drawn to guide the eye.

(see Table S1 in Supporting Information for an attribution of peaks according to symmetry).[75] For an orientative estimate, the prescriptions by Szafranski et al.[73] for roughened gold electrodes would project a decrease of average tilt angle of the aromatic ring from 26 to 21° with respect to the normal. In addition, the sharp rise of vibrational modes at 1372 and 1593 cm^{-1} suggests the onset of charge transfer from gold to MBT,[76−78] which points to a net change of surface electronic states (see also Figure S1 in Supporting Information). Meanwhile, the weak SERS bands associated with PEG that are visible in sample PEG/MBT 1:0 tend to disappear, which is consistent with a change of conformation that makes PEG more extended outward[79] or the onset of dynamic thiol exchange. PEG is the most popular choice to enhance the colloidal stability of particles intended for biomedical applications[51,60−62] and its loss may trigger flocculative processes.[80] However, we never observed any sign of flocculation, that is, no increase of hydrodynamic size, broadening of the plasmonic bands,[81] nor sedimentation, and we found consistent values of hydrodynamic size for all three samples. These qualitative observations collectively point to some persistence of PEG. Another detail discernible from our SERS spectra is the lack of clear Raman signals from CTAB[82,83] (see Figure S2 in Supporting Information), which is a cytotoxic surfactant used in the synthesis of gold nanorods. The presence of CTAB is a critical issue for the translation of gold nanorods into biomedical applications, and its thorough removal is a recurrent subject of research.[84−87] In this respect, our single-step protocol for PEGylation and purification in an acetate buffer containing polysorbate 20 is an efficient solution, consistent with our previous findings on the biological profiles of our particles.[51]

Thermal Stability. In order to verify the effect of MBT on the thermal stability of gold nanorods, we used an oven set at 90 °C and followed the shift of their plasmonic bands over time. We chose this temperature for no particular reason but to accelerate all kinetics without the nuisance of a boiling medium.

The upper left panel of Figure 2 shows the spectra of optical extinction of PEGylated particles left at 90 °C for different times. The longitudinal band blue shifts from 1144 to 998 nm after 1 h and then more slowly drifts to 970 nm after 2 h. In order to reconstruct the underlying transformation, we analyzed all spectra with the numerical model based on Mie-Gans theory, which allows us to translate the distribution of optical modes into one of shape.[25] The plasmonic shift corresponds to a modification of the distribution of AR from 7.7 ± 0.8 to 6.3 ± 0.6 after 1 h to 6.0 ± 0.6 after 2 h. The transmission electron micrographs reported in Supporting Information corroborate the validity of this interpretation, and reveal additional details. Upon annealing, the overall shape of the particles becomes smoother, that is, side-walls get flatter

https://dx.doi.org/10.1021/acs.jpcc.0c00737
J. Phys. Chem. C XXXX, XXX, XXX−XXX

and end-caps get rounder. The loss of AR derives more from an increase in diameter than a decrease in length, so that the average size of the particles seems to grow as in the presence of collective effects, such as Ostwald ripening[88] or coalescence. The possibility of Ostwald ripening has been evoked by previous authors in the presence of a large excess of surfactant,[26] or in the case of ultrasmall particles,[27] and will be the subject of our future investigation. The overall dynamics closely resemble the transformation of so-called gold nanodogbones that we found in a poly(vinyl alcohol) film heated to 110 °C[25] or of PEGylated gold nanorods constrained in an epoxy resin left at 120 to 220 °C,[24] that is, a rather sharp transition followed by a slow stabilization to a smoother intermediate between the initial shape and the spherical limit. Meanwhile, the fraction of spherical particles returned by our optical analysis did not increase over time (see Figure S3 in Supporting Information), which is in disagreement with a mechanism of spheroidization driven by Rayleigh-Plateau instability.

In this context, MBT exerts a significant stabilization of the initial shape. Figure 2 summarizes all optical results together with their decryption in morphological terms. The kind of rapid development that occurs around 45 min for PEGylated particles sets on around 90 min in sample PEG/MBT 1:1 and after more than 2 h in sample PEG/MBT 1:20. For instance, after 1 h at 90 °C, the rearrangement of AR from 7.7 ± 0.8 to 6.3 ± 0.6 seen in sample PEG/MBT 1:0 reduces to 7.5 ± 0.8 in sample PEG/MBT 1:1 and only 7.6 ± 0.8 in 1:20. After 2 h, the drift to 6.0 ± 0.6 in sample PEG/MBT 1:0 compares with 6.0 ± 0.8 in sample PEG/MBT 1:1 and 7.0 ± 0.8 in 1:20. In practice, after 1 h sample PEG/MBT 1:0 lost more than 70% of optical absorbance at its initial peak position, while 1:1 retained more than 96% and 1:20 retained more than 99%. We may say that sample PEG/MBT 1:0 already transitioned but the other two did not. After 2 h, sample PEG/MBT 1:0 lost more than 80%, 1:1 lost more than 70%, while 1:20 still retained more than 70%. Therefore, samples PEG/MBT 1:0 and 1:1 transitioned but 1:20 just began. According to our SERS data, no significant modification in the arrangement of the shell occurred in sample PEG/MBT 1:20 until 150 min of thermal treatment (see Figure S6 in Supporting Information), and so the onset of the deformation does not seem to originate from the desorption of MBT. We hypothesize that the density of facets and defects in gold nanorods grown at ambient conditions may raise the stability of the adsorbate.[89]

From a technological perspective, the conditions applied in the thermal treatment of our samples are too severe to simulate major cases as the optical hyperthermia of cancer, where the typical combination of temperature and time is much milder, and PEGylated gold nanorods are quite enough.[2,3,33,61] However, in other emerging contexts, such as the use of plasmonic particles in biochemical processes as the polymerase chain reaction,[90−92] our results may make a substantial impact (see Supporting Information).

We hypothesize that the effect of MBT delays the process of premelting and stabilizes the initial shape through the interplay of different factors. One possible factor is chemical coordination,[30−32] as it determines the difference between subsurface and surface diffusivity as well as more subtle effects, such as the relative stability of rounder rods.[22,24] Another relevant factor is the stiffness of the environment,[21,24] which is regarded as the main player involved in alternative strategies as silanization.[14,18,24,33] We suggest that the adsorption of small thiols may synergistically affect both aspects, that is, gold coordination and adlayer stiffness, with a high density of surface atoms tightly pinned to an aromatic shell cooperatively hardened by the effect of π-stacking.[42−45,48] A similar mechanism was already invoked to explain the effect of small thiols on the mechanical strength of nanoporous gold.[93] The steric crowdedness of the organic shell may be another element playing against a loss of surface to volume ratio, as was proposed in the case of polymers as PEG.[24] Previous authors have predicted[31] and observed[26,27] that a weak adsorbate may enhance the thermal stability of ultrathin gold nanowires and rods by retarding their surface atom diffusivity, and that a stronger and stabler interaction may enhance this effect. Our work suggests that a dense layer of aromatic thiols may represent a viable solution to fulfill this objective. Finally, we emphasize that different elements of our results prove to be very robust and were confirmed in different batches of gold nanorods prepared from the same or alternative synthetic protocols (see Supporting Information): that PEGylated particles undergo a thermal transformation over a few tens of minutes around 90 °C that settles to an intermediate shape between the initial one and the spherical limit and that MBT stabilizes the initial shape and delays its deformation easily by a factor around 3 in time.

Stability of Photoacoustic Conversion. In order to challenge the versatility of our concept in a context of more practical relevance and more established solutions, we verified the use of MBT to enhance the stability of photoacoustic conversion of gold nanorods suspended in an aqueous medium. Here, we exploited a microfluidic setup[57] to monitor the intensity of the photoacoustic signal versus the fluence of the optical trigger set at a wavelength of 1064 nm. The typical outcome is a linear behavior that persists until the onset of a sublinearity related to a photoinstability.[57,94] Indeed, the slope of the curve corresponds to the efficiency of photoacoustic conversion, which starts to decrease as the subpopulation of particles that resonate with the optical trigger begins to reshape within the time scale of each pulse. The regime at play is very different from the previous conditions, that is, a time scale in the order of few nanoseconds or shorter, peak temperature up to several hundreds of centigrades,[15,16] and optical selectivity for the subpopulation of particles with the appropriate shape and instantaneous orientation.[95,96] However, it is understood that the underlying process is the same, that is, overheating and premelting[22,23] with the possibility of additional photomechanical effects.[50] Figure 3 displays our results.

In order to analyze our results, we fitted the experimental curves to an empirical model that is the product of a linear trend times a sigmoid function[18,23] describing the depletion of optical absorbance of the particles. Regardless of the theoretical justification of this model, its use provides an excellent description of the experimental data, and a quantitative tool to identify the onset of the sublinearity. Figure 3b shows the optical fluence that corresponds to a level of loss of efficiency of photoacoustic conversion of 25% of the initial value, consistent with our previous gauge.[16,18,23] We found an increase from (15 ± 3) mJ/cm^2 for our PEGylated benchmark to (19 ± 4) mJ/cm^2 for sample PEG/MBT 1:1 to (30 ± 6) mJ/cm^2 for 1:20. The effect of MBT in sample PEG/MBT 1:20 is also evident on visual inspection, and amounts to a doubling of damage threshold, which brings our particles to approach relevant MPE limits in the near-infrared window of biological tissue.[20] This result is rather surprising, when it is

https://dx.doi.org/10.1021/acs.jpcc.0c00737
J. Phys. Chem. C XXXX, XXX, XXX−XXX

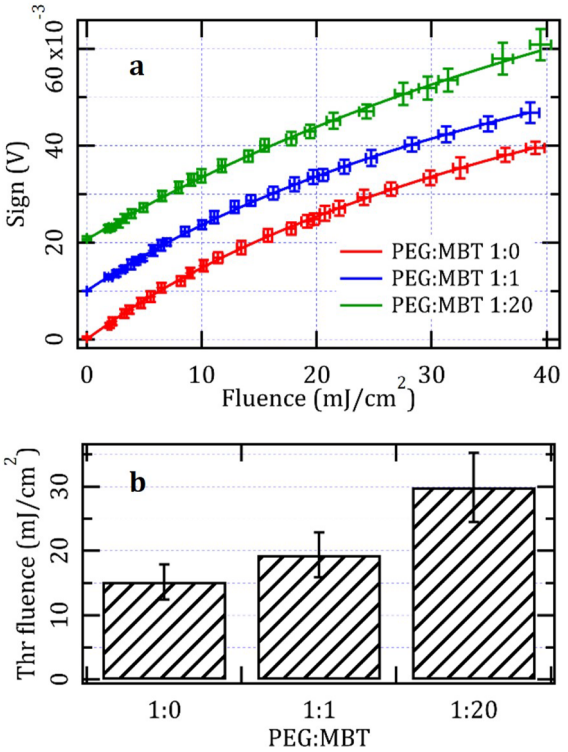

Figure 3. (a) Photoacoustic signal as a function of fluence of the optical trigger for particles prepared with the named mixtures of thiols: dots are experimental values; lines are a fit to an analytical model that accounts for a depletion of optical absorbance. (b) Threshold of fluence of the optical trigger corresponding to a loss of efficiency of photoacoustic conversion by 25%.

considered that an increase of damage threshold by 100% is what we predicted for a shell of organosilica as thick as 10 nm.[18] We hypothesize that the elasticity and self-healing capacity[97,98] of a dense layer of MBT supporting the deformation and reformation of intermolecular noncovalent interactions[99] may provide an advantage with respect to a brittle glass as organosilica, where eventual failure probably relates to a photomechanical event of irreversible rupture. In this regime of optical excitation, the effect of density seems to be more prominent than the case of simple annealing at 90 °C for reasons that may belong to the cooperative resistance of the monolayer against desorption.[42−45,48]

CONCLUSIONS

In conclusion, we have investigated the effect of an aromatic thiol as MBT on the thermal and photostability of gold nanorods. We have treated colloidal suspensions of gold nanorods with mixtures of thiolated PEG and MBT with different molar ratios ranging from pure PEG to PEG/MBT 1:20. During annealing in an oven set at 90 °C, we found a sharp effect of MBT to delay the deformation of gold nanorods, for example, from 45 min to beyond 2 h. For instance, whereas after 1 h particles with PEG alone lost more than 70% of optical absorbance at their initial peak position, those saturated with MBT remained nearly unchanged. This result may enable the introduction of gold nanorods in biochemical processes as the polymerase chain reaction that require thermal annealing at temperatures approaching the boiling point of water over tens of minutes. In addition, we addressed the effect of MBT on the photostability of gold nanorods irradiated under conditions of interest for photoacoustic imaging. Also, in this case we found a delay of relevant damage thresholds by about a factor of 2, that is, from 15 to 30 mJ/cm^2, which becomes comparable with MPE constraints at a wavelength of 1064 nm.

In the future, we will address the extension of our findings to other models of small mono-, di-, and multivalent thiols, including the effect of a higher density of thiolated PEG,[86,87] binary or more complex mixtures, cofactors, or more kinds of soft templates, in order to understand their generality and to pursue their optimization for real-world applications. We are confident that our results will inspire more work to overcome the limitations related to the thermal and photostability of plasmonic tags.

ASSOCIATED CONTENT

Supporting Information

The Supporting Information is available free of charge at https://pubs.acs.org/doi/10.1021/acs.jpcc.0c00737.

SERS data, additional details; thermal stability of PEGylated gold nanorods, morphological details; thermal stability of MBT-modified gold nanorods, applications in the polymerase chain reaction; thermal stability of MBT-modified gold nanorods, persistence of the shell (PDF)

AUTHOR INFORMATION

Corresponding Author

Fulvio Ratto − *Istituto di Fisica Applicata "Nello Carrara", Consiglio Nazionale delle Ricerche, 50019 Sesto Fiorentino (FI), Italy;* orcid.org/0000-0001-6721-9486; Phone: +39 0555225307; Email: f.ratto@ifac.cnr.it

Authors

Sonia Centi − *Istituto di Fisica Applicata "Nello Carrara", Consiglio Nazionale delle Ricerche, 50019 Sesto Fiorentino (FI), Italy*

Lucia Cavigli − *Istituto di Fisica Applicata "Nello Carrara", Consiglio Nazionale delle Ricerche, 50019 Sesto Fiorentino (FI), Italy;* orcid.org/0000-0002-6279-8869

Claudia Borri − *Istituto di Fisica Applicata "Nello Carrara", Consiglio Nazionale delle Ricerche, 50019 Sesto Fiorentino (FI), Italy*

Alessio Milanesi − *Istituto di Fisica Applicata "Nello Carrara", Consiglio Nazionale delle Ricerche, 50019 Sesto Fiorentino (FI), Italy; Dipartimento di Chimica "Ugo Schiff", Universitá degli Studi di Firenze, 50019 Sesto Fiorentino (FI), Italy*

Martina Banchelli − *Istituto di Fisica Applicata "Nello Carrara", Consiglio Nazionale delle Ricerche, 50019 Sesto Fiorentino (FI), Italy*

Sofia Chioccioli − *Dipartimento di Biologia, Universitá degli Studi di Firenze, 50019 Sesto Fiorentino (FI), Italy*

Boris N. Khlebtsov − *Institute of Biochemistry and Physiology of Plants and Microorganisms, Russian Academy of Sciences, Saratov 410049, Russia;* orcid.org/0000-0003-3996-5750

Nikolai G. Khlebtsov − *Institute of Biochemistry and Physiology of Plants and Microorganisms, Russian Academy of Sciences, Saratov 410049, Russia; Saratov State University, Saratov 410026, Russia;* orcid.org/0000-0002-2055-7784

Paolo Matteini − *Istituto di Fisica Applicata "Nello Carrara", Consiglio Nazionale delle Ricerche, 50019 Sesto Fiorentino (FI), Italy;* orcid.org/0000-0002-8488-5867

https://dx.doi.org/10.1021/acs.jpcc.0c00737
J. Phys. Chem. C XXXX, XXX, XXX−XXX

Patrizia Bogani − *Dipartimento di Biologia, Universitá degli Studi di Firenze, 50019 Sesto Fiorentino (FI), Italy*
Roberto Pini − *Istituto di Fisica Applicata "Nello Carrara", Consiglio Nazionale delle Ricerche, 50019 Sesto Fiorentino (FI), Italy*

Complete contact information is available at: https://pubs.acs.org/10.1021/acs.jpcc.0c00737

Notes

The authors declare no competing financial interest.

■ ACKNOWLEDGMENTS

This work was partially supported by a collaborative grant from National Research Council Italy and Russian Foundation for Basic Research (18-52-7803, "HYPNOSYs") and by Regione Toscana within Project "SENSOGM".

■ REFERENCES

(1) Hu, M.; Chen, J.; Li, Z.-Y.; Au, L.; Hartland, G. V.; Li, X.; Marquez, M.; Xia, Y. Gold Nanostructures: Engineering Their Plasmonic Properties for Biomedical Applications. *Chem. Soc. Rev.* **2006**, *35*, 1084−1094.
(2) Jain, P. K.; Huang, X.; El-Sayed, I. H.; El-Sayed, M. A. Noble Metals on the Nanoscale: Optical and Photothermal Properties and Some Applications in Imaging, Sensing, Biology, and Medicine. *Acc. Chem. Res.* **2008**, *41*, 1578−1586.
(3) Huang, X.; Neretina, S.; El-Sayed, M. A. Gold Nanorods: From Synthesis and Properties to Biological and Biomedical Applications. *Adv. Mater.* **2009**, *21*, 4880−4910.
(4) Dreaden, E. C.; Alkilany, A. M.; Huang, X.; Murphy, C. J.; El-Sayed, M. A. The Golden Age: Gold Nanoparticles for Biomedicine. *Chem. Soc. Rev.* **2012**, *41*, 2740−2779.
(5) Dykman, L.; Khlebtsov, N. Gold Nanoparticles in Biomedical Applications: Recent Advances and Perspectives. *Chem. Soc. Rev.* **2012**, *41*, 2256−2282.
(6) Dykman, L. A.; Khlebtsov, N. G. Gold Nanoparticles in Chemo-, Immuno-, and Combined Therapy: Review [Invited]. *Biomed. Opt. Express* **2019**, *10*, 3152−3182.
(7) Kim, K.; Huang, S.-W.; Ashkenazi, S.; O'Donnell, M.; Agarwal, A.; Kotov, N. A.; Denny, M. F.; Kaplan, M. J. Photoacoustic Imaging of Early Inflammatory Response Using Gold Nanorods. *Appl. Phys. Lett.* **2007**, *90*, 223901.
(8) Wang, L. V. Multiscale Photoacoustic Microscopy and Computed Tomography. *Nat. Photonics* **2009**, *3*, 503−509.
(9) Lu, W.; Huang, Q.; Ku, G.; Wen, X.; Zhou, M.; Guzatov, D.; Brecht, P.; Su, R.; Oraevsky, A.; Wang, L. V.; et al. Photoacoustic Imaging of Living Mouse Brain Vasculature Using Hollow Gold Nanospheres. *Biomaterials* **2010**, *31*, 2617−2626.
(10) Li, P.-C.; Huang, S.-W.; Wei, C.-W.; Chiou, Y.-C.; Chen, C.-D.; Wang, C.-R. C. Photoacoustic Flow Measurements by Use of Laser-Induced Shape Transitions of Gold Nanorods. *Opt. Lett.* **2005**, *30*, 3341−3343.
(11) Zharov, V. P.; Galanzha, E. I.; Shashkov, E. V.; Khlebtsov, N. G.; Tuchin, V. V. In Vivo Photoacoustic Flow Cytometry for Monitoring of Circulating Single Cancer Cells and Contrast Agents. *Opt. Lett.* **2006**, *31*, 3623−3625.
(12) Pérez-Juste, J.; Rodríguez-González, B.; Mulvaney, P.; Liz-Marzán, L. Optical Control and Patterning of Gold-Nanorod−Poly(vinyl alcohol) Nanocomposite Films. *Adv. Funct. Mater.* **2005**, *15*, 1065−1071.
(13) Petrova, H.; Perez Juste, J.; Pastoriza-Santos, I.; Hartland, G. V.; Liz-Marzán, L. M.; Mulvaney, P. On the Temperature Stability of Gold Nanorods: Comparison Between Thermal and Ultrafast Laser-Induced Heating. *Phys. Chem. Chem. Phys.* **2006**, *8*, 814−821.
(14) Chen, Y.-S.; Frey, W.; Kim, S.; Homan, K.; Kruizinga, P.; Sokolov, K.; Emelianov, S. Enhanced Thermal Stability of Silica-Coated Gold Nanorods for Photoacoustic Imaging and Image-Guided Therapy. *Opt. Express* **2010**, *18*, 8867−8878.
(15) Chen, X.; Chen, Y.; Yan, M.; Qiu, M. Nanosecond Photothermal Effects in Plasmonic Nanostructures. *ACS Nano* **2012**, *6*, 2550−2557.
(16) Cavigli, L.; de Angelis, M.; Ratto, F.; Matteini, P.; Rossi, F.; Centi, S.; Fusi, F.; Pini, R. Size Affects the Stability of the Photoacoustic Conversion of Gold Nanorods. *J. Phys. Chem. C* **2014**, *118*, 16140−16146.
(17) Moon, H.; Kumar, D.; Kim, H.; Sim, C.; Chang, J.-H.; Kim, J.-M.; Kim, H.; Lim, D.-K. Amplified Photoacoustic Performance and Enhanced Photothermal Stability of Reduced Graphene Oxide Coated Gold Nanorods for Sensitive Photoacoustic Imaging. *ACS Nano* **2015**, *9*, 2711−2719.
(18) Lai, S.; Centi, S.; Borri, C.; Ratto, F.; Cavigli, L.; Micheletti, F.; Kemper, B.; Ketelhut, S.; Kozyreva, T.; Gonnelli, L.; et al. A Multifunctional Organosilica Cross-Linker for the Bio-Conjugation of Gold Nanorods. *Colloids Surf., B* **2017**, *157*, 174−181.
(19) Chen, Y.-S.; Zhao, Y.; Yoon, S. J.; Gambhir, S. S.; Emelianov, S. Miniature Gold Nanorods for Photoacoustic Molecular Imaging in the Second Near-Infrared Optical Window. *Nat. Nanotechnol.* **2019**, *14*, 465−472.
(20) *American National Standard for Safe Use of Lasers*; Laser-Institute of America, ANSI: New York, 2014.
(21) Zhang, Q.; Xia, Z.; Cheng, Y.-B.; Gu, M. High-Capacity Optical Long Data Memory Based on Enhanced Young's Modulus in Nanoplasmonic Hybrid Glass Composites. *Nat. Commun.* **2018**, *9*, 1183.
(22) Taylor, A. B.; Siddiquee, A. M.; Chon, J. W. M. Below Melting Point Photothermal Reshaping of Single Gold Nanorods Driven by Surface Diffusion. *ACS Nano* **2014**, *8*, 12071−12079.
(23) Cavigli, L.; Cini, A.; Centi, S.; Borri, C.; Lai, S.; Ratto, F.; de Angelis, M.; Pini, R. Photostability of Gold Nanorods upon Endosomal Confinement in Cultured Cells. *J. Phys. Chem. C* **2017**, *121*, 6393−6400.
(24) Kennedy, W. J.; Izor, S.; Anderson, B. D.; Frank, G.; Varshney, V.; Ehlert, G. J. Thermal Reshaping Dynamics of Gold Nanorods: Influence of Size, Shape, and Local Environment. *ACS Appl. Mater. Interfaces* **2018**, *10*, 43865−43873.
(25) Ratto, F.; Matteini, P.; Cini, A.; Centi, S.; Rossi, F.; Fusi, F.; Pini, R. CW Laser-Induced Photothermal Conversion and Shape Transformation of Gold Nanodogbones in Hydrated Chitosan Films. *J. Nanopart. Res.* **2011**, *13*, 4337−4348.
(26) Zou, R.; Zhang, Q.; Zhao, Q.; Peng, F.; Wang, H.; Yu, H.; Yang, J. Thermal Stability of Gold Nanorods in an Aqueous Solution. *Colloids Surf., A* **2010**, *372*, 177−181.
(27) Takahata, R.; Yamazoe, S.; Warakulwit, C.; Limtrakul, J.; Tsukuda, T. Rayleigh Instability and Surfactant-Mediated Stabilization of Ultrathin Gold Nanorods. *J. Phys. Chem. C* **2016**, *120*, 17006−17010.
(28) Nichols, F. A.; Mullins, W. W. Surface (Interface) and Volume Diffusion Contributions to Morphological Changes Driven by Capillarity. *Trans. Metal. Soc. AIME* **1965**, *233*, 1840−1847.
(29) Karim, S.; Toimil-Molares, M. E.; Balogh, A. G.; Ensinger, W.; Cornelius, T. W.; Khan, E. U.; Neumann, R. Morphological Evolution of Au Nanowires Controlled by Rayleigh Instability. *Nanotechnology* **2006**, *17*, 5954−5959.
(30) Jaklevic, R. C.; Elie, L. Scanning-Tunneling-Microscope Observation of Surface Diffusion on an Atomic Scale: Au on Au(111). *Phys. Rev. Lett.* **1988**, *60*, 120−123.
(31) Huber, S. E.; Warakulwit, C.; Limtrakul, J.; Tsukuda, T.; Probst, M. Thermal Stabilization of Thin Gold Nanowires by Surfactant-Coating: A Molecular Dynamics Study. *Nanoscale* **2012**, *4*, 585−590.
(32) He, X.; Cheng, F.; Chen, Z. The Lattice Kinetic Monte Carlo Simulation of Atomic Diffusion and Structural Transition for Gold. *Sci. Rep.* **2016**, *6*, 33128.
(33) Moreira, A. F.; Rodrigues, C. F.; Reis, C. A.; Costa, E. C.; Correia, I. J. Gold-Core Silica Shell Nanoparticles Application in

Imaging and Therapy: A Review. *Microporous Mesoporous Mater.* **2018**, *270*, 168−179.
(34) Mazzoni, M.; Dagar, J.; Lai, S.; Centi, S.; Ratto, F.; Pini, R.; Zani, L. Transformed Double-Capped Gold Nanorods in Dye Co-Sensitized Solar Cells for Semitransparent Windows. *Curr. Nanosci.* **2019**, *15*, 309−318.
(35) Yang, X.; Liu, X.; Liu, Z.; Pu, F.; Ren, J.; Qu, X. Near-Infrared Light-Triggered, Targeted Drug Delivery to Cancer Cells by Aptamer Gated Nanovehicles. *Adv. Mater.* **2012**, *24*, 2890−2895.
(36) Zhang, Z.; Wang, L.; Wang, J.; Jiang, X.; Li, X.; Hu, Z.; Ji, Y.; Wu, X.; Chen, C. Mesoporous Silica-Coated Gold Nanorods as a Light-Mediated Multifunctional Theranostic Platform for Cancer Treatment. *Adv. Mater.* **2012**, *24*, 1418−1423.
(37) Huang, Y.; Rosei, F.; Vetrone, F. A Single Multifunctional Nanoplatform Based on Upconversion Luminescence and Gold Nanorods. *Nanoscale* **2015**, *7*, 5178−5185.
(38) Love, J. C.; Estroff, L. A.; Kriebel, J. K.; Nuzzo, R. G.; Whitesides, G. M. Self-Assembled Monolayers of Thiolates on Metals as a Form of Nanotechnology. *Chem. Rev.* **2005**, *105*, 1103−1170.
(39) Jadzinsky, P. D.; Calero, G.; Ackerson, C. J.; Bushnell, D. A.; Kornberg, R. D. Structure of a Thiol Monolayer-Protected Gold Nanoparticle at 1.1 Å Resolution. *Science* **2007**, *318*, 430−433.
(40) Vericat, C.; Vela, M. E.; Benitez, G.; Carro, P.; Salvarezza, R. C. Self-Assembled Monolayers of Thiols and Dithiols on Gold: New Challenges for a Well-Known System. *Chem. Soc. Rev.* **2010**, *39*, 1805−1834.
(41) Schlenoff, J. B.; Li, M.; Ly, H. Stability and Self-Exchange in Alkanethiol Monolayers. *J. Am. Chem. Soc.* **1995**, *117*, 12528−12536.
(42) Murty, K. V. G. K.; Venkataramanan, M.; Pradeep, T. Self-assembled Monolayers of 1,4-Benzenedimethanethiol on Polycrystalline Silver and Gold Films: An Investigation of Structure, Stability, Dynamics, and Reactivity. *Langmuir* **1998**, *14*, 5446−5456.
(43) Bandyopadhyay, K.; Vijayamohanan, K.; Venkataramanan, M.; Pradeep, T. Self-Assembled Monolayers of Small Aromatic Disulfide and Diselenide Molecules on Polycrystalline Gold Films: A Comparative Study of the Geometrical Constraint Using Temperature-Dependent Surface-Enhanced Raman Spectroscopy, X-ray Photoelectron Spectroscopy, and Electrochemistry. *Langmuir* **1999**, *15*, 5314−5322.
(44) Wan, L.-J.; Terashima, M.; Noda, H.; Osawa, M. Molecular Orientation and Ordered Structure of Benzenethiol Adsorbed on Gold(111). *J. Phys. Chem. B* **2000**, *104*, 3563−3569.
(45) Garg, N.; Carrasquillo-Molina, E.; Lee, T. R. Self-Assembled Monolayers Composed of Aromatic Thiols on Gold: Structural Characterization and Thermal Stability in Solution. *Langmuir* **2002**, *18*, 2717−2726.
(46) Cristina, L. J.; Ruano, G.; Salvarezza, R.; Ferròn, J. Thermal Stability of Self-Assembled Monolayers of n-Hexanethiol on Au(111)-(1 × 1) and Au(001)-(1 × 1). *J. Phys. Chem. C* **2017**, *121*, 27894−27904.
(47) Rittikulsittichai, S.; Park, C. S.; Jamison, A. C.; Rodriguez, D.; Zenasni, O.; Lee, T. R. Bidentate Aromatic Thiols on Gold: New Insight Regarding the Influence of Branching on the Structure, Packing, Wetting, and Stability of Self-Assembled Monolayers on Gold Surfaces. *Langmuir* **2017**, *33*, 4396−4406.
(48) Verwüster, E.; Wruss, E.; Zojer, E.; Hofmann, O. T. Exploring the Driving Forces Behind the Structural Assembly of Biphenylthiolates on Au(111). *J. Chem. Phys.* **2017**, *147*, 024706.
(49) Vigderman, L.; Zubarev, E. R. High-Yield Synthesis of Gold Nanorods with Longitudinal SPR Peak Greater than 1200 nm Using Hydroquinone as a Reducing Agent. *Chem. Mater.* **2013**, *25*, 1450−1457.
(50) Cavigli, L.; Centi, S.; Borri, C.; Tortoli, P.; Panettieri, I.; Streit, I.; Ciofini, D.; Magni, G.; Rossi, F.; Siano, S.; et al. 1064-nm-Resonant Gold Nanorods for Photoacoustic Theranostics Within Permissible Exposure Limits. *J. Biophotonics* **2019**, *12*, e201900082.
(51) Tatini, F.; Landini, I.; Scaletti, F.; Massai, L.; Centi, S.; Ratto, F.; Nobili, S.; Romano, G.; Fusi, F.; Messori, L.; et al. Size Dependent Biological Profiles of PEGylated Gold Nanorods. *J. Mater. Chem. B* **2014**, *2*, 6072−6080.
(52) Centi, S.; Tatini, F.; Ratto, F.; Gnerucci, A.; Mercatelli, R.; Romano, G.; Landini, I.; Nobili, S.; Ravalli, A.; Marrazza, G. In Vitro Assessment of Antibody-Conjugated Gold Nanorods for Systemic Injections. *J. Nanobiotechnol.* **2014**, *12*, 55.
(53) Pérez-Juste, J.; Pastoriza-Santos, I.; Liz-Marzán, L. M.; Mulvaney, P. Gold Nanorods: Synthesis, Characterization and Applications. *Coord. Chem. Rev.* **2005**, *249*, 1870−1901.
(54) Ratto, F.; Witort, E.; Tatini, F.; Centi, S.; Lazzeri, L.; Carta, F.; Lulli, M.; Vullo, D.; Fusi, F.; Supuran, C. T.; et al. Plasmonic Particles that Hit Hypoxic Cells. *Adv. Funct. Mater.* **2015**, *25*, 316−323.
(55) Khlebtsov, B.; Khanadeev, V.; Pylaev, T.; Khlebtsov, N. A New T-Matrix Solvable Model for Nanorods: TEM-Based Ensemble Simulations Supported by Experiments. *J. Phys. Chem. C* **2011**, *115*, 6317−6323.
(56) Matteini, P.; Cottat, M.; Tavanti, F.; Panfilova, E.; Scuderi, M.; Nicotra, G.; Menziani, M. C.; Khlebtsov, N.; de Angelis, M.; Pini, R. Site-Selective Surface-Enhanced Raman Detection of Proteins. *ACS Nano* **2017**, *11*, 918−926.
(57) Cavigli, L.; Micheletti, F.; Tortoli, P.; Centi, S.; Lai, S.; Borri, C.; Rossi, F.; Ratto, F.; Pini, R. *Light Activated Microbubbles for Imaging and Microsurgery* **2017**, *10064*, 744−750.
(58) Nedosekin, D. A.; Fahmi, T.; Nima, Z. A.; Nolan, J.; Cai, C.; Sarimollaoglu, M.; Dervishi, E.; Basnakian, A.; Biris, A. S.; Zharov, V. P. Photoacoustic Flow Cytometry for Nanomaterial Research. *Photoacoustics* **2017**, *6*, 16−25.
(59) Frigenti, G.; Cavigli, L.; Fernández-Bienes, A.; Ratto, F.; Centi, S.; García-Fernández, T.; Nunzi Conti, G.; Soria, S. Resonant Microbubble as a Microfluidic Stage for All-Optical Photoacoustic Sensing. *Phys. Rev. Appl.* **2019**, *12*, 014062.
(60) Niidome, T.; Yamagata, M.; Okamoto, Y.; Akiyama, Y.; Takahashi, H.; Kawano, T.; Katayama, Y.; Niidome, Y. PEG-Modified Gold Nanorods with a Stealth Character for in Vivo Applications. *J. Controlled Release* **2006**, *114*, 343−347.
(61) von Maltzahn, G.; Park, J.-H.; Agrawal, A.; Bandaru, N. K.; Das, S. K.; Sailor, M. J.; Bhatia, S. N. Computationally Guided Photothermal Tumor Therapy Using Long-Circulating Gold Nanorod Antennas. *Cancer Res.* **2009**, *69*, 3892−3900.
(62) Centi, S.; Ratto, F.; Tatini, F.; Lai, S.; Pini, R. Ready-to-Use Protein G-Conjugated Gold Nanorods for Biosensing and Biomedical Applications. *J. Nanobiotechnol.* **2018**, *16*, 5.
(63) Nara, J.; Higai, S.; Morikawa, Y.; Ohno, T. Density Functional Theory Investigation of Benzenethiol Adsorption on Au(111). *J. Chem. Phys.* **2004**, *120*, 6705−6711.
(64) Seo, K.; Borguet, E. Potential-Induced Structural Change in a Self-Assembled Monolayer of 4-Methylbenzenethiol on Au(111). *J. Phys. Chem. C* **2007**, *111*, 6335−6342.
(65) Kuzumoto, Y.; Kitamura, M. Work Function of Gold Surfaces Modified Using Substituted Benzenethiols: Reaction Time Dependence and Thermal Stability. *Appl. Phys. Express* **2014**, *7*, 035701.
(66) Zeng, C.; Chen, Y.; Kirschbaum, K.; Lambright, K. J.; Jin, R. Emergence of Hierarchical Structural Complexities in Nanoparticles and Their Assembly. *Science* **2016**, *354*, 1580−1584.
(67) Banchelli, M.; Amicucci, C.; Ruggiero, E.; D'Andrea, C.; Cottat, M.; Ciofini, D.; Osticioli, I.; Ghini, G.; Siano, S.; Pini, R.; et al. Spot-on SERS Detection of Biomolecules with Laser-Patterned Dot Arrays of Assembled Silver Nanowires. *ChemNanoMat* **2019**, *5*, 1036−1043.
(68) Khlebtsov, B. N.; Bratashov, D. N.; Khlebtsov, N. G. Tip-Functionalized Au@Ag Nanorods as Ultrabright Surface-Enhanced Raman Scattering Probes for Bioimaging in Off-Resonance Mode. *J. Phys. Chem. C* **2018**, *122*, 17983−17993.
(69) Khlebtsov, B. N.; Bratashov, D. N.; Byzova, N. A.; Dzantiev, B. B.; Khlebtsov, N. G. SERS-Based Lateral Flow Immunoassay of Troponin I by Using Gap-Enhanced Raman Tags. *Nano Res.* **2019**, *12*, 413−420.
(70) Rycenga, M.; Xia, X.; Moran, C. H.; Zhou, F.; Qin, D.; Li, Z.-Y.; Xia, Y. Generation of Hot Spots with Silver Nanocubes for Single-

https://dx.doi.org/10.1021/acs.jpcc.0c00737
J. Phys. Chem. C XXXX, XXX, XXX−XXX

Molecule Detection by Surface-Enhanced Raman Scattering. *Angew. Chem., Int. Ed.* **2011**, *50*, 5473−5477.
(71) Lu, G.; Shrestha, B.; Haes, A. J. Importance of Tilt Angles of Adsorbed Aromatic Molecules on Nanoparticle Rattle SERS Substrates. *J. Phys. Chem. C* **2016**, *120*, 20759−20767.
(72) Carron, K. T.; Hurley, L. G. Axial and Azimuthal Angle Determination with Surface-Enhanced Raman Spectroscopy: Thiophenol on Copper, Silver, and Gold Metal Surfaces. *J. Phys. Chem.* **1991**, *95*, 9979−9984.
(73) Szafranski, C. A.; Tanner, W.; Laibinis, P. E.; Garrell, R. L. Surface-Enhanced Raman Spectroscopy of Aromatic Thiols and Disulfides on Gold Electrodes. *Langmuir* **1998**, *14*, 3570−3579.
(74) Holze, R. The Adsorption of Thiophenol on Gold − a Spectroelectrochemical Study. *Phys. Chem. Chem. Phys.* **2015**, *17*, 21364−21372.
(75) Varsányi, G.; Láng, L. *Assignments for Vibrational Spectra of Seven Hundred Benzene Derivatives*; Wiley: New York, 1974.
(76) Yoon, J. H.; Park, J. S.; Yoon, S. Time-Dependent and Symmetry-Selective Charge-Transfer Contribution to SERS in Gold Nanoparticle Aggregates. *Langmuir* **2009**, *25*, 12475−12480.
(77) Ye, J.; Hutchison, J. A.; Uji-i, H.; Hofkens, J.; Lagae, L.; Maes, G.; Borghs, G.; Van Dorpe, P. Excitation Wavelength Dependent Surface Enhanced Raman Scattering of 4-Aminothiophenol on Gold Nanorings. *Nanoscale* **2012**, *4*, 1606−1611.
(78) Goldmann, C.; Lazzari, R.; Paquez, X.; Boissière, C.; Ribot, F.; Sanchez, C.; Chanéac, C.; Portehault, D. Charge Transfer at Hybrid Interfaces: Plasmonics of Aromatic Thiol-Capped Gold Nanoparticles. *ACS Nano* **2015**, *9*, 7572−7582.
(79) Levin, C. S.; Bishnoi, S. W.; Grady, N. K.; Halas, N. J. Determining the Conformation of Thiolated Poly(ethylene glycol) on Au Nanoshells by Surface-Enhanced Raman Scattering Spectroscopic Assay. *Anal. Chem.* **2006**, *78*, 3277−3281.
(80) Niidome, T.; Ohga, A.; Akiyama, Y.; Watanabe, K.; Niidome, Y.; Mori, T.; Katayama, Y. Controlled Release of PEG Chain from Gold Nanorods: Targeted Delivery to Tumor. *Bioorg. Med. Chem.* **2010**, *18*, 4453−4458.
(81) Mazzoni, M.; Ratto, F.; Fortunato, C.; Centi, S.; Tatini, F.; Pini, R. Partial Decoupling in Aggregates of Silanized Gold Nanorods. *J. Phys. Chem. C* **2014**, *118*, 20018−20025.
(82) Zhang, Z.; Lin, M. Fast Loading of PEG−SH on CTAB-Protected Gold Nanorods. *RSC Adv.* **2014**, *4*, 17760−17767.
(83) Tebbe, M.; Kuttner, C.; Männel, M.; Fery, A.; Chanana, M. Colloidally Stable and Surfactant-Free Protein-Coated Gold Nanorods in Biological Media. *ACS Appl. Mater. Interfaces* **2015**, *7*, 5984−5991.
(84) Leonov, A. P.; Zheng, J.; Clogston, J. D.; Stern, S. T.; Patri, A. K.; Wei, A. Detoxification of Gold Nanorods by Treatment with Polystyrenesulfonate. *ACS Nano* **2008**, *2*, 2481−2488.
(85) Boca, S. C.; Astilean, S. Detoxification of Gold Nanorods by Conjugation with Thiolated Poly(ethylene glycol) and Their Assessment as SERS-Active Carriers of Raman Tags. *Nanotechnology* **2010**, *21*, 235601.
(86) Kinnear, C.; Dietsch, H.; Clift, M. J. D.; Endes, C.; Rothen-Rutishauser, B.; Petri-Fink, A. Gold Nanorods: Controlling Their Surface Chemistry and Complete Detoxification by a Two-Step Place Exchange. *Angew. Chem., Int. Ed.* **2013**, *52*, 1934−1938.
(87) Ruff, J.; Steitz, J.; Buchkremer, A.; Noyong, M.; Hartmann, H.; Besmehn, A.; Simon, U. Multivalency of PEG-Thiol Ligands Affects the Stability of NIR-Absorbing Hollow Gold Nanospheres and Gold Nanorods. *J. Mater. Chem. B* **2016**, *4*, 2828−2841.
(88) Voorhees, P. W. The Theory of Ostwald Ripening. *J. Stat. Phys.* **1985**, *38*, 231−252.
(89) Cortés, E.; Rubert, A. A.; Benitez, G.; Carro, P.; Vela, M. E.; Salvarezza, R. C. Enhanced Stability of Thiolate Self-Assembled Monolayers (SAMs) on Nanostructured Gold Substrates. *Langmuir* **2009**, *25*, 5661−5666.
(90) Li, M.; Lin, Y.-C.; Wu, C.-C.; Liu, H.-S. Enhancing the Efficiency of a PCR Using Gold Nanoparticles. *Nucleic Acids Res.* **2005**, *33*, e184−e184.
(91) Vanzha, E.; Pylaev, T.; Khanadeev, V.; Konnova, S.; Fedorova, V.; Khlebtsov, N. Gold Nanoparticle-Assisted Polymerase Chain Reaction: Effects of Surface Ligands, Nanoparticle Shape and Material. *RSC Adv.* **2016**, *6*, 110146−110154.
(92) Roche, P. J. R.; Najih, M.; Lee, S. S.; Beitel, L. K.; Carnevale, M. L.; Paliouras, M.; Kirk, A. G.; Trifiro, M. A. Real Time Plasmonic qPCR: How Fast is Ultra-Fast? 30 Cycles in 54 Seconds. *Analyst* **2017**, *142*, 1746−1755.
(93) Mameka, N.; Lührs, L.; Heissler, S.; Gliemann, H.; Wöll, C. Tailoring the Strength of Nanoporous Gold by Self-Assembled Monolayers of Alkanethiols. *ACS Appl. Nano Mater.* **2018**, *1*, 6613−6621.
(94) Knights, O. B.; Ye, S.; Ingram, N.; Freear, S.; McLaughlan, J. R. Optimising Gold Nanorods for Photoacoustic Imaging in Vitro. *Nanoscale Adv.* **2019**, *1*, 1472−1481.
(95) Zijlstra, P.; Chon, J. W. M.; Gu, M. Five-Dimensional Optical Recording Mediated by Surface Plasmons in Gold Nanorods. *Nature* **2009**, *459*, 410−3.
(96) Zharov, V. P. Ultrasharp Nonlinear Photothermal and Photoacoustic Resonances and Holes Beyond the Spectral Limit. *Nat. Photonics* **2011**, *5*, 110−116.
(97) Rybtchinski, B. Adaptive Supramolecular Nanomaterials Based on Strong Noncovalent Interactions. *ACS Nano* **2011**, *5*, 6791−6818.
(98) Meltzer, C.; Paul, J.; Dietrich, H.; Jäger, C. M.; Clark, T.; Zahn, D.; Braunschweig, B.; Peukert, W. Indentation and Self-Healing Mechanisms of a Self-Assembled Monolayer—A Combined Experimental and Modeling Study. *J. Am. Chem. Soc.* **2014**, *136*, 10718−10727.
(99) Tuncaboylu, D. C.; Sari, M.; Oppermann, W.; Okay, O. Tough and Self-Healing Hydrogels Formed via Hydrophobic Interactions. *Macromolecules* **2011**, *44*, 4997−5005.

https://dx.doi.org/10.1021/acs.jpcc.0c00737
J. Phys. Chem. C XXXX, XXX, XXX−XXX